Investigation of Size-Dependent Plasmonic and Catalytic Properties of Metallic Nanocrystals Enabled by Size Control with HCl Oxidative Etching

*Bo Li, Ran Long, Xiaolan Zhong, Yu Bai, Zijie Zhu, Xing Zhang, Min Zhi, Jiawei He, Chengming Wang, Zhi-Yuan Li, and Yujie Xiong**

***P**article size is one important parameter of nanocrystals that need to be tightly controlled, owing to its versatility for tailoring the properties and functions of nanocrystals towards various applications. In this article, oxidative etching by hydrogen chloride is employed as a tool to control the size of metallic nanocrystals. As a result of the size control, investigations into the size-dependent plasmonic and catalytic properties of metallic nanocrystals can be investigated. Given that the shape can be kept consistent when tuning the particle size in this system, it enables the systematic investigation of size-dependent properties free of the influence of other factors such as shape effect.*

1. Introduction

In rational design of material functionality, particle size is one of the most important parameters that need to be tightly controlled, as it allows tailoring the properties of nanocrystals towards various applications.[1] For example, surface plasmonic features of silver and gold nanocrystals are very sensitive to their sizes;[2] catalytic activities of palladium nanocatalysts can be ideally enhanced when downscaling their dimensions.[3] For this reason, considerable efforts have been made to control the size of metallic nanocrystals in various synthetic systems. Thus the size-dependent properties of nanocrystals can be fully investigated.

One of the mostly used methods for size control is to stop reactions and take samples out of the reaction solution at different stages of nanocrystal growth.[4] This enables facilely achieving size control in a certain range of particle sizes; however, the geometrical shapes of nanocrystals may have a very large inconsistency in the early stages of crystal growth, which may significantly modify their properties in terms of shape effect.[4b] More importantly, this method cannot make full use of raw chemicals due to low conversion yield, when stopping reactions in a short period of time for synthesizing nanocrystals in small sizes. An alternative is the seeding scheme where particle size is maneuvered by controllably adding metal atoms onto the surface of seeds.[5] Despite the complexity of the two-step process, this method is generally limited by the low concentrations of seeds and chemicals that are required for the seeding process, which in turn yields very small amounts of products. Overall, it is necessary to develop a new method for producing size-tunable nanocrystals at high yield and in consistent geometrical shapes. To this end, Xia and Xiong developed an oxidative etching method for palladium synthesis where Fe(III) species were added as an etchant into the reduction of palladium precursors.[6] The oxidative etchant could oxidize newly formed palladium atoms back to $[PdCl_4]^{2-}$ ions in the synthesis. This oxidation

B. Li,[+] R. Long,[+] Y. Bai, Z. Zhu, X. Zhang, M. Zhi, J. He, C. Wang, Prof. Y. Xiong
Hefei National Laboratory for Physical Sciences at the Microscale
University of Science and Technology of China
Jinzhai Road 96, Hefei, Anhui 230026, P. R. China
E-mail: yjxiong@ustc.edu.cn
X. Zhong, Prof. Z.-Y. Li
Beijing National Laboratory for Condensed Matter Physics
Institute of Physics
Chinese Academy of Sciences
P.O. Box 603, Beijing 100190, P. R. China
[+] B.L. and R.L. contributed equally to this work.

DOI: 10.1002/smll.201200243

small NANO MICRO

of the freshly generated palladium atoms competed with the reduction of palladium precursor $[PdCl_4]^{2-}$, and thus made the reduction substantially slow. The tight control over the reduction kinetics in turn led to the nucleation of palladium atoms into nuclei at a relatively low rate.[6] This manipulation over nucleation can effectively reduce the number of nuclei and thus increase the size of final particles, given that the concentration of palladium precursor is fixed. The strategy of implementing oxidative etching in controlling the particle size should be generic to multiple systems; however, the etchant of Fe(III) species is not applicable to other metal systems due to different potentials of metals. For instance, in the case of silver, Fe(III) species can actually scavenge the oxygen in solution and diminish the role of oxidative etching in removing twinned structures, eventually leading to the formation of silver nanowires.[7]

In this article, we demonstrate the use of hydrogen chloride (HCl) as an effective etchant for size control. This method can be generically applied to multiple metal systems and shapes. The original motivation of using HCl comes from the inevitable presence of chloride ions in reaction solution in the polyol process—the mostly used synthetic system for metallic nanocrystals.[7] Chloride is an impurity involved from the manufacture of ethylene glycol (with typical amounts ≤1–3 ppm), and the inconsistent concentration of this impurity makes the synthesis not very reproducible.[8] Since the presence of chloride cannot be easily eliminated from the reaction system, we shall develop a method to overwrite its influence on the synthesis, and at the same time, make use of chloride to achieve size control. Herein, we demonstrate that we can tune the size of silver and palladium nanocrystals in both cubic and cuboctahedral shapes by HCl etching. In this method, the shapes of metallic nanocrystals can be kept consistent when tuning the particle size, allowing investigating the size-dependent plamsonic and catalytic properties free of the influence from other factors such as shape effect.

2. Results and Discussion

Our initial investigation is based on a synthetic system for silver nanocubes developed by Xia research group recently.[4] It includes ethylene glycol as both solvent and reducing agent, silver trifluoroacetate (CF_3COOAg) as silver precursor, and sodium hydrosulfide (NaHS) as a catalyst precursor. In our synthesis, HCl is added as an etchant for oxidative etching, whose concentration can basically overwrite the effect of chloride impurity from ethylene glycol. All the samples were collected at 3 h when the reactions were completed. The conversion yield of precursors into nanoparticles was over 90% in all the syntheses, as determined by inductively coupled plasma mass spectrometry (ICP-MS). The identical yield of each synthesis provides a platform for investigating the correlation of amounts of etchants (that determines the number of nuclei) with final particle size. **Figure 1** shows typical scanning and transmission electron microscopy (SEM and TEM) images of three samples prepared in the presence of HCl at different concentrations ranging from 0.21 to 0.35 mM. This set of concentrations is much higher than the amount of

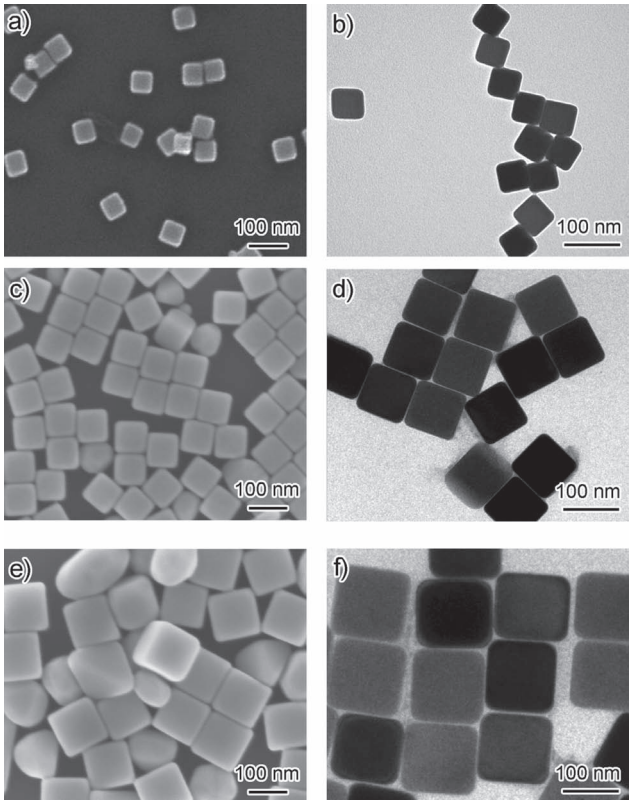

Figure 1. SEM and TEM images of silver nanocubes prepared in presence of different amounts of HCl showing the effect of etching on particle size: a,b) 0.21; c,d) 0.28, and e,f) 0.35 mM.

chloride in the used ethylene glycol (≤2 ppm; i.e., ≤0.055 mM), so the influence from the chloride impurities can be overwritten. The images reveal that more than 90% nanoparticles have cubic shape and their sizes are turned from 54 to 86 nm and then 126 nm when increasing the concentration of HCl. The calculation based on the particle size and synthesis yield indicates that the increase of particle size mainly works through the reduction of number of nuclei due to the oxidative etching induced by HCl (see Figure S1, Supporting Information (SI)). Note that the dependence of particle size on HCl concentrations is very reproducible: we used three different batches of ethylene glycol in our synthesis (Aladdin, ≤2 ppm chloride; Sigma-Aldrich, ≤ 3 ppm chloride; J. T. Baker, ≤1 ppm chloride), and obtained similarly sized Ag nanocubes. Thus we can also conclude that this synthesis does not suffer the reproducibility issue of many polyol syntheses that was caused by the impurities of chloride.

Further investigation indicates that HCl oxidative etching actually plays dual functions in the synthesis. At a lower concentration of HCl (0.14 mM, see Figure S2a,b in the SI), the size of resulted nanoparticles is decreased to 40 nm as expected; however, a significant amount of twinned structures can be found in the product. The emergence of twinned structure is very common in the system of silver.[9] The size window that favors both silver icosahedrons and decahedrons is much broader than with other metals, as silver has the lowest energy barrier for incorporating stacking faults.[1] As a result, twinned structures are commonly recognized

in silver products. Previous studies have shown that defect zones in twinned seeds are much higher in energy relative to single-crystal counterparts and thus are most susceptible to an oxidative environment. Their atoms can be attacked by the etchant, oxidized and dissolved into the solution, removing twinned structures from the final products.[8c,9] Thus the oxidative etching induced by HCl can prevent the formation of twinned structures in the present work. As such, when oxidative etching is strong enough at a certain concentration of HCl, twinned structures cannot be generated, leaving high-purity single-crystal nanocubes in the final products. Figure S3 (SI) shows the TEM images of the sample collected from the early stage of the synthesis (at about 25 min) in the presence of 0.21 mM HCl, identifying that a significant amount of twinned structures was generated in initial stages. However, the twinned structures could be etched away when the reaction progressed (as compared with Figure 1b for reaction time 3 h). This observation clearly confirms the first function of oxidative etching in the synthesis–removing the twinned seeds. Apparently, 0.14 mM HCl is not sufficient to provide etching function for eliminating the growth of twinned seeds. The second function of oxidative etching here is to oxidize newly formed silver atoms back to ions in the synthesis and thus make the reduction of precursors slower. We have measured the concentrations of unreacted silver precursors using ICP-MS in the reaction timeframe of 0–4 min (see Figure S4, SI). From the measurements, we recognized that the amounts of unreacted Ag(I) decreased in the first 1 min due to nucleation but then transiently increased in the next 1 min. The increase of Ag(I) concentration in reaction solution indicates that oxidative etching on newly formed silver atoms should have occurred in the reaction. In addition, we observed that the amounts of silver atoms etched back to silver ions are dependent on the concentrations of added HCl. Thus oxidative etching should be the main factor responsible for the kinetic control in the reduction of silver precursors. The kinetic control of reduction enables the manipulation over the nucleation rate of silver atoms and in turn the number of nuclei. Given that the concentration of silver precursors is fixed in each synthesis, the size of final particles can be tuned with varied number of nuclei. Note that oxidative etching only occurred on the freshly generated silver atoms rather than on the formed nanocubes, as indicated by the UV–vis spectra of nanoparticles produced at different stages (Figure S5, SI).

In the present case, the oxidative etching mainly works through oxygen in reaction solution but incorporation of corrosive ions such as chloride can greatly enhance its capability of attacking atomic metals on surface.[10] The Cl^-/O_2 pair has been used as a versatile etchant in the synthesis of metallic nanocrystals in the past years; however, it has been proven not powerful enough to achieve a relatively large scope of control in terms of the two etching functions aforementioned. **Figure 2**a shows a typical image of the sample prepared in the presence of 0.35 mM NaCl (a concentration of Cl^- equivalent to that in Figure 1e). It reveals that twinned structures are the major products, indicating that oxidative etching by Cl^-/O_2 pair alone is not strong enough to remove twinned seeds.

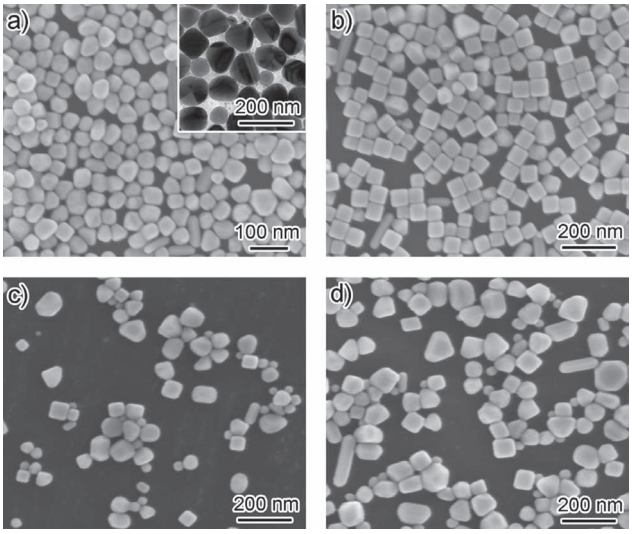

Figure 2. SEM images of silver nanocrystals prepared in presence of different amounts of NaCl showing the role of chloride in the synthesis: a) 0.35, b) 0.70, c) 1.05, and d) 1.40 mM. The inset of a shows a TEM image of the sample in a.

Although twinned seeds can be etched by further increasing the concentration of NaCl, the tunable size range is relatively narrow as compared with the synthesis using HCl. This limitation mainly comes from the possibility of producing AgCl precipitates at a high concentration of chloride (see Figure 2b–d).

The acidic nature of HCl can greatly enhance the strength of oxidative etching and thus make the window of size control broader, according to the standard electrical potentials:[8d,11]

$$O_2 + 4H^+ + 4e^- \rightarrow 2H_2O \quad E^0 = 1.229V$$

$$O_2 + 2H_2O + 4e^- \rightarrow 4OH^- \quad E^0 = 0.401V$$

The function of acid has been proved by control experiments. Figure S6 (SI) shows SEM images of the samples obtained with a combination of 0.35 mM NaCl with varied amounts of CF_3COOH. The morphologies of samples are gradually turned from twinned structures to single-crystal nanocubes, implying that the oxidative etching can be enhanced with the addition of acid. Certainly acid alone cannot induce appropriate etching and remove twinned structures, as indicated by the reactions using CF_3COOH instead of HCl (see Figure S7, SI).

The size of silver nanocubes has a strong correlation with the concentration of HCl through the function of oxidative etching (see Figure S8, SI), whereas the addition of excessive HCl will lead to production of silver nanowires and right bipyramids (see Figure S2c,d (SI)). This appearance of twinned structures is ascribed to the formation of intermediate AgCl as the concentration of Cl^- reaches a certain threshold. As indicated in literature, the intermediate of silver halide tends to form planar stacking faults in final nanocrystals.[12] The presence of a planar defect can form concave surfaces on one side where newly formed atoms

small NANO MICRO

can be easily added to grow along one or two dimensions, causing the production of five-fold nanowires or single-twinned structures such as right bipyramids. The experiments with excessive amounts of NaCl (Figure 2c,d) also confirm the formation of twinned structures at a high concentration of Cl^-. Figure S9 (SI) shows some experiments by varying the concentration of Cl^- while the acidic condition is kept the same. The products mainly consist of nanocubes with the addition of 0.21 mM CF_3COOH and 0.21 mM NaCl, but they became to form more nanowires by increasing the amount of NaCl. It verifies that chloride is the main contributor to turn the synthesis into the production of silver nanowires at an extremely high concentration of HCl, implying that formation of twinned structures in Figure S2c (SI) can be ascribed to the intermediate of AgCl.

The tunable size of silver nanocubes in the present work offers an opportunity for investigating size-dependent localized surface plasmon resonance (LSPR) properties experimentally. **Figure 3**a gives UV–vis spectra taken from aqueous suspensions of the silver nanocrystals depicted in Figure 1 and Figure S1 (SI), clearly showing that the LSPR band was continuously red-shifted as the particle size increases. The major LSPR peak of 40-nm nanoparticles is located at 430 nm, which can be assigned to dipole resonance.[13] In comparison, there are two additional distinct peaks in the LSPR band of 54-nm nanocubes despite the red-shift of major peak to 464 nm due to size effect: one at 350 nm (weak dipole) and the other at 379 nm (quadrupole) whose emergence can be ascribed to the relatively low symmetry of cubic shape as compared to nearly spherical 40-nm nanoparticles.[14] As the size of nanocubes further increases to 86 nm, the dipole peak is tuned to 535 nm while a new peak appears at 445 nm. This newly appearing peak can be indexed to quadrupole resonance whose contribution generally promotes with the increase of particle size.[13] When the size approaches 126 nm, the quadrupole peak at 506 nm becomes the dominant one in the overall extinction spectrum curve, and the entire LSPR band continues red-shifting. Figure 3b shows extinction coefficients of silver nanocubes in the corresponding sizes as calculated using the discrete dipole approximation (DDA) method. The LSPR features in simulation are fairly consistent with those observed in our experiments. The intensity ratios between peaks are slightly different from those observed experimentally, which could result from the slight truncation of our synthesized nanocubes. The tunable LSPR features make it interesting to use these silver nanocubes as substrates for surface-enhanced Raman scattering (SERS) detection.[15] Figure 3c compares the SERS spectra of 1,4-benzenedithiol (1,4-BDT) adsorbed on the surfaces of silver nanocubes at these three different sizes. The spectra were recorded from aqueous suspensions with roughly the same particle concentration. Based on the phenyl ring stretching mode at 1562 cm^{-1},[16] the SERS enhancement factors (EFs) were estimated as 2.65×10^5, 4.64×10^5, and 7.69×10^4 for the 54-, 86-, and 126-nm nanocubes, respectively. Different from the previous results,[5] our data show a relatively big variation in EFs when tuning the particle size. Past studies have confirmed the notion that the most intense SERS is generally observed when the surface plasmon of a nanoparticle is in resonance with the incident radiation.[8d,15,17] In our SERS experiments, we used a laser with the wavelength of 514 nm. Given that the dipole peak of 86-nm nanocubes is located at 535 nm (versus

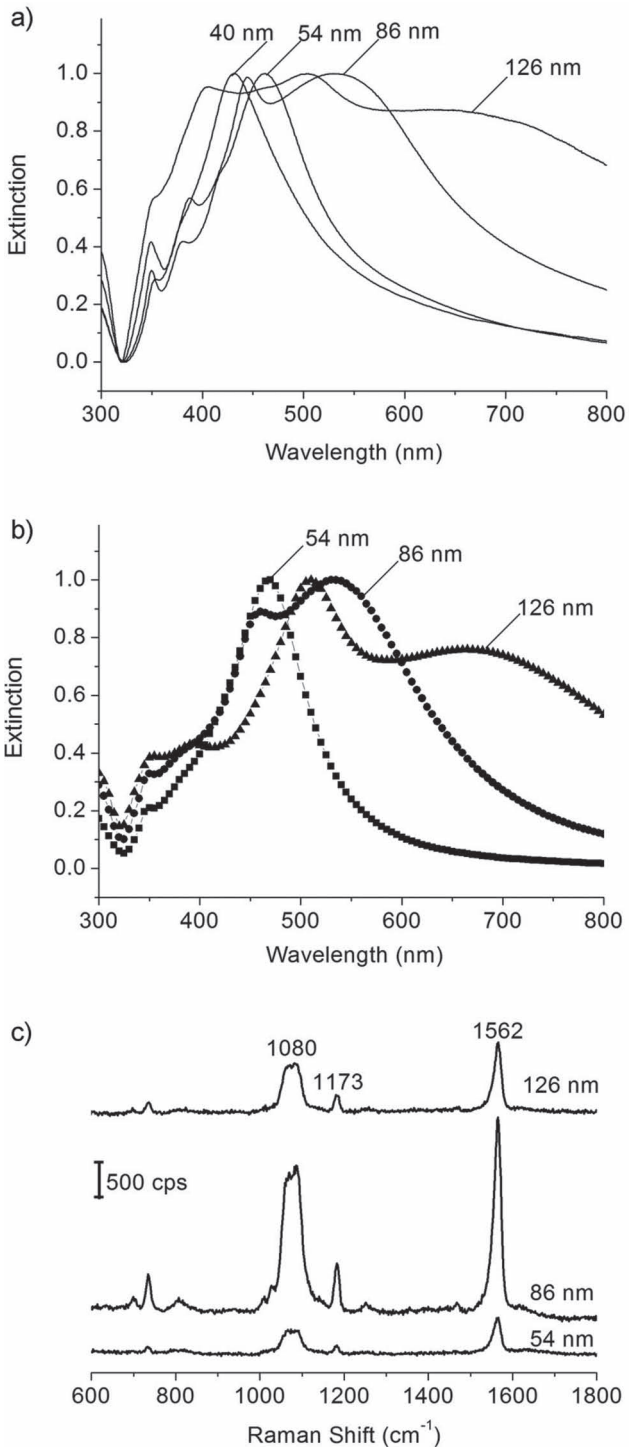

Figure 3. a) UV–vis spectra of aqueous suspensions of silver nanoparticles in different sizes. b) SPR spectra of silver nanocubes in different sizes calculated by DDA method. c) Solution-phase SERS spectra of 1,4-BDT adsorbed on silver nanocubes in different sizes. All samples were suspended in water and the suspensions had the same particle concentrations. The SERS spectra were recorded with an excitation wavelength of λ_{ex} = 514 nm and a laser power of P_{laser} = 6.8 mW for a period of t = 60 s.

464 nm for 54-nm nanocubes and a very broad LSPR band for 126-nm nanocubes), the SERS enhancement should be the strongest for 86-nm silver nanocubes. Thus it is believed that this EF difference mainly comes from the tunable LSPR features of silver nanocubes.

Thanks to the generic features of this approach, the use of HCl as an etchant can be applied to other metals and shapes. For instance, we have employed this method for tuning the size of palladium nanocubes. Chloride is a type of ions that are included in various reaction systems, such as that in K_2PdCl_4—a commonly used precursor for synthesizing palladium nanocrystals. Thus the addition of HCl into the reactions would not increase the complexity of reaction systems. In the synthesis of palladium nanocubes, we have confirmed the role of oxidative etching by HCl by measuring the concentrations of unreacted palladium precursors using UV–vis spectroscopy in the reaction timeframe of 0–6 min (see Figure S10, SI). Similar to the silver case, we observed the transient increase of palladium precursor concentrations between 2 and 4 min, indicating the role of HCl in etching newly formed palladium atoms back to ions. Moreover, it revealed that the reduction rate of palladium precursors became lower when HCl was added, implying that oxidative etching had successfully slowed the reduction kinetics of palladium. It is worth pointing out that the role of HCl in the palladium and in the silver cases is not totally identical, although they share a similar mechanism in terms of oxidative etching induced by HCl. The main difference in these two systems comes from the following factors: i) chloride can form AgCl precipitates with silver ions when the concentration of added HCl reaches a certain threshold, so the amount of HCl added to the silver synthesis cannot be as high as that used in the palladium case; ii) the acidity of HCl may slightly affect the reducing ability of L-ascorbic acid used in the palladium synthesis, but this effect should be very minimal according to the kinetic measurement using HBr instead of HCl. Despite the difference between the two systems, the oxidative etching induced by HCl can still provide a powerful tool for the size control of palladium nanocrystals. **Figure 4**a–d shows TEM images of palladium nanocubes with their sizes tuned by the concentration of HCl, based on a synthetic method that we developed a few years ago.[18] By increasing the HCl concentration, the size of nanocubes has been successfully tailored from 8 to 20 nm. Moreover, HCl can serve as an etchant to tune the size of other metal nanostructures. Figure 4e,-f shows that the function of size tuning by HCl can be also used in the synthesis of palladium cuboctahedrons with a capability of handling the size range from 5 to 20 nm.

Enabled by the size control of palladium nanocubes, we investigated the size dependence of palladium nanocrystals on their catalytic properties in organic reactions. In this investigation, we employed the oxidation of 3,5,3′,5′-tetramethylbenzidine (TMB), an aromatic amine, as a model system for catalytic comparison. This reaction has been widely used as a chromogenic substrate in staining procedures in immunohistochemistry as well as a visualizing reagent used in enzyme-linked immunosorbent assays.[19] TMB can react with peroxidase enzymes and yield colored products through the pathway as shown in Figure S11 (SI). The absorption

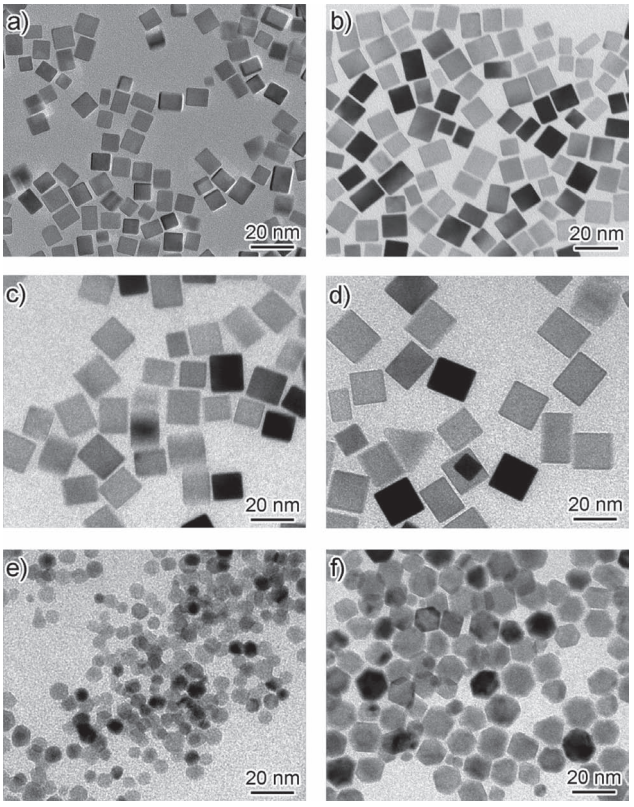

Figure 4. TEM images of palladium nanocubes prepared in the presence of HCl at different concentrations: a) 0, b) 21.8, c) 60, and d) 109 mM. TEM images of palladium cuboctahedrons prepared in the presence of HCl at different concentrations: e) 0 and f) 218 mM.

wavelengths of one-electron oxidation intermediate (cation free-radical) and two-electron oxidation product (diimine) are located at 370 nm/652 nm and 450 nm, respectively.[19] In general, peroxide is a necessary component for this oxidation reaction; however, we found that TMB molecules could be oxidized to colored products when they were mixed with palladium nanocrystals in the absence of peroxides. The reaction rates catalyzed by palladium nanocubes exhibited much higher than that by hydrogen peroxide at 10 °C. Figure S12 (SI) shows a photograph of a TMB solution mixed with various materials that clearly resolves the color change trend. Surprisingly, 20-nm palladium nanocubes showed higher activity than 8-nm counterparts, although it is commonly considered that catalytic activities of nanoparticles should be improved by downscaling their dimensions. **Figure 5**a,b shows UV–vis spectra of TMB solution in the presence of 8- and 20-nm nanocubes, respectively. From the spectra, it reveals that 20-nm nanocubes converted most TMB molecules into final products of diimine in 1 h while a considerable amount of molecules was maintained at the intermediate stage of cation free-radicals treated with 8-nm nanocubes. The results imply that palladium nanocubes with different sizes can catalyze the reaction probably by efficiently generating oxygen radicals (O^-, O_2^-, or O_3^-) from oxygen dissolved in water but exhibit varied catalytic activities. To capture oxygen radicals generated by palladium nanocubes, we have employed 5,5-dimethyl-1-pyrroline

small NANO MICRO

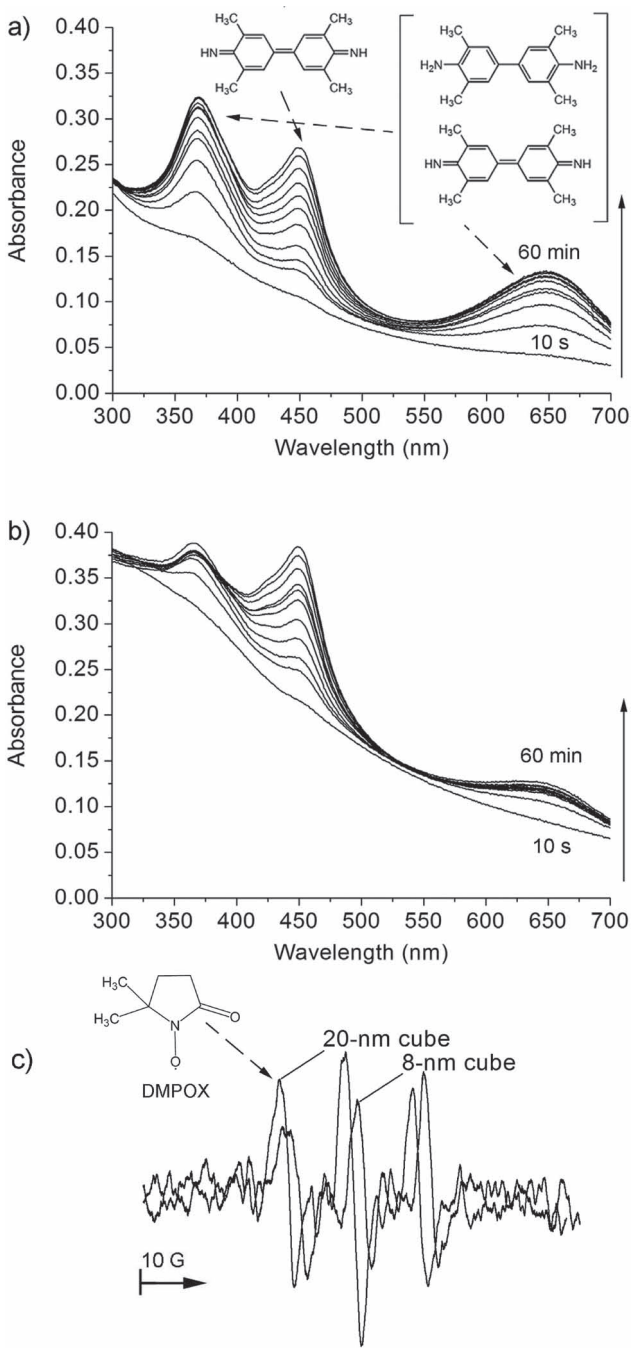

Figure 5. UV–vis spectra of the samples after mixing TMB solution with palladium nanocubes in different sizes: a) 8 and b) 20 nm. c) ESR spectra of the samples after mixing DMPO solution with palladium nanocubes in different sizes.

N-oxide (DMPO) as a detecting agent that can interact with oxygen radicals and undergo a series of reactions as shown in Figure S13 (SI).[20] The intermediate and final products were analyzed with the electron spin resonance (ESR) spectroscopy, showing that no obvious signals from O_2^- radicals were obtained in the ESR spectra (Figure 5c). We suspect that oxygen radicals transiently emerged in the reactions so that they could not be captured by ESR in a very short period of time. Another possibility is that oxygen species were in other forms of oxygen radicals such as O^- and O_3^- that could not be trapped by DMPO molecules. However, we observed the signals from 5,5-dimethyl-1-pyrrolidone-2-oxyl (DMPOX) in the presence of palladium nanocubes, indicating that oxygen radicals were generated in the system indeed. The signals for large nanocubes are slightly stronger than those for small ones, so we can speculate that their varied performance in the TMB reaction should be ascribed to different capability of producing oxygen radicals. Note that we have conducted the TMB reaction catalyzed in different gas environment, further confirming that oxygen is necessary for the reaction process. So we can conclude that the TMB reaction carried out through the generation of oxygen species. Overall, clear variation in catalysis for organic reactions has been observed while tuning the particle size. Since oxygen radicals are commonly involved in various organic reactions, it is anticipated that size control would provide a versatile tool to design related heterogeneous catalysts. In the future, we will conduct further investigations on detailed surface characterizations and corresponding theoretical simulation which can provide more information for elucidating the mechanism why size increase can promote the generation of oxygen radicals in organic reactions.

3. Conclusion

In summary, we have developed a method for tuning the size of metallic nanocrystals by employing oxidative etching with HCl. As chloride is a component that cannot be eliminated from the polyol process and other syntheses with metal chlorides involved, the use of HCl in the present method represents a facile route for the controlled synthesis of metallic nanocrystals. Given that the shape can be kept consistent when tuning the particle size in our system, it enables the systematic investigation of size-dependent properties free of the influence of shape effect. As a result, we have successfully observed size-dependent plasmonic and catalytic properties. From the side of synthesis, the dependence of particle size on the HCl concentration also provides some insights, indicating that we should never overlook minor factors in a synthesis, as a slight change—such as the addition of trace HCl—may bring huge variation in the morphology of final products.

4. Experimental Section

Size Control of Silver Nanocubes: The synthetic procedure is similar to that in literature, but the amount of HCl is adjusted for controlling oxidative etching.[4a] In a typical synthesis, ethylene glycol (50 mL, EG, Aladdin, 1095698-500 mL) was added into a 250-mL round bottom flask and heated under magnetic stirring in an oil bath preset to 150 °C. NaSH (0.6 mL, 3 mM in EG, Sigma-Aldrich, 02326AH) was quickly injected into the heated solution after its temperature had reached 150 °C. After 2 min, a HCl solution (5 mL) was injected into the reaction solution, followed by the addition of poly(vinyl pyrrolidone) (PVP, 12.5 mL, 20 mg/mL in EG,

molecular weight, M.W. = 55–000, Sigma-Aldrich, 856568-100g). The HCl solution was prepared by adding different amounts of HCl (38% by weight) into EG. After another 2 min, silver trifluoroacetate (4 mL, 282 mM in EG, Sigma-Aldrich, 04514TH) was added into the mixture. The reaction mixture was heated at 150 °C in air for 3 h. The samples were washed with acetone and then with ethanol and water several times to remove most of the EG and PVP by centrifugation. The as-obtained samples were then characterized by SEM and TEM.

Size Control of Palladium Nanocubes: The synthetic procedure is similar to that we developed previously but different amounts of HCl is added for oxidative etching.[16] In a typical synthesis, and PVP (0.105 g, M.W. = 55 000), KBr (0.300 g) and L-ascorbic acid (0.060 g, Sigma-Aldrich, A0278-25g) were dissolved in deionized water (8 mL) at room temperature. The solution was placed in a 3-neck flask (equipped with a reflux condenser and a magnetic Teflon-coated stirring bar) and heated in air at 80 °C for 10 min. Meanwhile, potassium palladium(II) chloride (K_2PdCl_4, 0.065 g, Aladdin, 1098844-1g) was dissolved in deionized water (3 mL) at room temperature. Subsequently, different amounts of HCl were added to the flask. Then the Pd stock solution was immediately injected into the flask. The reaction mixture was heated at 80 °C in air for 3 h.

Size Control of Palladium Cuboctahedrons: In a typical synthesis, PVP (0.105 g, M.W. = 55 000), citric acid (0.060 g, Sigma-Aldrich, 251275-100g) and L-ascorbic acid (0.060 g) were dissolved in deionized water (8 mL) at room temperature. The solution was placed in a 3-neck flask (equipped with a reflux condenser and a magnetic Teflon-coated stirring bar) and heated in air at 120 °C for 5 min. Meanwhile, K_2PdCl_4 (0.065 g) was dissolved in deionized water (3 mL) at room temperature. Subsequently, different amounts of HCl were added to the flask. Then the Pd stock solution was immediately injected into the flask. Heating of the reaction at 120 °C was continued in air for 3 h.

SERS Measurements: The Ag nanocubes were functionalized with an ethanol solution of 1,4-BDT (1 mM) over a period of 2 h. Ethanol was used to wash the sample several times before the particles were re-dispersed in water to obtain a concentration of 0.5 nM in terms of particles. The Raman spectra were recorded from the suspension using a JY LABRAM-HR micro-Raman spectrophotometer. The SERS data were collected with λ_{ex} = 514 nm, P_{laser} = 6.8 mW, and t = 60 s. The solution samples were contained in a home-made cell for Raman measurements.

TMB Measurements: 3,5,3′,5′-tetramethylbenzidine aqueous solution (20 μL, 50 mM) was mixed with HAc/NaAc buffer solution (2 mL, 0.2 M:0.2 M). An aqueous suspension of different palladium nanocrystals (50 μL, 0.2 mg/mL) was then added into the mixture solution at 10 °C. The samples were taken at different time for UV–vis measurements. UV–vis absorption spectra were collected using an Agilent Varien Cary 60 spectrophotometer.

DMPO Measurements: An aqueous suspension of different palladium nanocrystals (50 μL, 0.75 mg/mL) was mixed with DMPO solution (500 μL, 50 mM). The solution was then characterized with a JES-FA200 electron spin resonance (ESR) spectroscopy at 20 °C.

Supporting Information

Supporting Information is available from the Wiley Online Library or from the author.

Acknowledgements

This work was financially supported by the National Natural Science Foundation of China (No. 21101145, 91123010, J1030412), the Recruitment Program of Global Experts, and the CAS Hundred Talent Program.

[1] Y. Xia, Y. Xiong, B. Lim, S. E. Skrabalak, *Angew. Chem. Int. Ed.* **2009**, *48*, 60.
[2] B. J. Wiley, S. H. Im, Z.-Y. Li, J. M. McLellan, A. Siekkinen, Y. Xia, *J. Phys. Chem. B* **2006**, *110*, 15666.
[3] M. Jin, H. Liu, H. Zhang, Z. Xie, J. Liu, Y. Xia, *Nano Res.* **2011**, *4*, 83.
[4] a) Q. Zhang, W. Li, L.-P. Wen, J. Chen, Y. Xia, *Chem. Eur. J.* **2010**, *16*, 10234; b) B. Wiley, T. Herricks, Y. Sun, Y. Xia, *Nano Lett.* **2004**, *4*, 1733.
[5] Q. Zhang, W. Li, C. Moran, J. Chen, L. Wen, Y. Xia, *J. Am. Chem. Soc.* **2010**, *132*, 11372.
[6] Y. Xiong, J. Chen, B. Wiley, Y. Xia, Y. Yin, Z.-Y. Li, *Nano Lett.* **2005**, *5*, 1237.
[7] B. Wiley, Y. Sun, Y. Xia, *Langmuir* **2005**, *21*, 8077.
[8] a) Y. Sun, Y. Xia, *Science* **2002**, *298*, 2176; b) F. Kim, S. Connor, H. Song, T. Kuykendall, P. Yang, *Angew. Chem. Int. Ed.* **2004**, *43*, 3673; c) Y. Xiong, J. Chen, B. Wiley, Y. Xia, S. Aloni, Y. Yin, *J. Am. Chem. Soc.* **2005**, *127*, 7332; d) Y. Xiong, J. M. McLellan, J. Chen, Y. Yin, Z.-Y. Li, Y. Xia, *J. Am. Chem. Soc.* **2005**, *127*, 17118.
[9] B. Wiley, T. Herricks, Y. Sun, Y. Xia, *Nano Lett.* **2004**, *4*, 1733.
[10] a) R. C. Newman, K. Sieradzki, *Science* **1994**, *263*, 1708; b) J. C. Scully, *The Fundamentals of Corrosion*, 3rd ed., Pergamon Press, Oxford, New York **1990**, 1–57; c) Y. Xiong, B. Wiley, J. Chen, Z.-Y. Li, Y. Yin, Y. Xia, *Angew. Chem. Int. Ed.* **2005**, *44*, 7913.
[11] *Handbook of Chemistry and Physics*, 60th ed. (Ed: R. C. Weast), CRC Press, Boca Raton, FL **1980**.
[12] C. Lofton, W. Sigmund, *Adv. Func. Mater.* **2005**, *15*, 1197.
[13] F. Zhou, Z.-Y. Li, Y. Liu, Y. Xia, *J. Phys. Chem. C* **2008**, *112*, 20233.
[14] Y. Xiong, *Chem. Commun.* **2011**, *47*, 1580.
[15] a) M. Rycenga, M. H. Kim, P. H. C. Camargo, C. Cobley, Z.-Y. Li, Y. Xia, *J. Phys. Chem. A* **2009**, *113*, 3932; b) M. Rycenga, C. M. Cobley, J. Zeng, W. Li, C. H. Moran, Q. Zhang, D. Qin, Y. Xia, *Chem. Rev.* **2011**, *111*, 3669.
[16] a) M. Osawa, N. Matsuda, K. Yoshii, I. Uchida, *J. Phys. Chem.* **1994**, *98*, 12702; b) J. Y. Gui, D. A. Stern, D. G. Frank, F. Lu, D. C. Zapien, A. T. Hubbard, *Langmuir* **1991**, *7*, 955.
[17] a) C. J. Orendorff, L. Gearheart, N. R. Jana, C. J. Murphy, *Phys. Chem. Chem. Phys.* **2006**, *8*, 165; b) Y. Yang, S. Matsubara, L. Xiong, T. Hayakawa, M. Nogami, *J. Phys. Chem. C* **2007**, *111*, 9095; c) J. B. Jackson, N. J. Halas, *Proc. Natl. Acad. Sci. USA* **2004**, *101*, 17930.
[18] Y. Xiong, H. Cai, B. J. Wiley, J. Wang, M. J. Kim, Y. Xia, *J. Am. Chem. Soc.* **2007**, *129*, 3665.
[19] P. D. Josephy, T. Eling, R. P. Mason, *J. Biol. Chem.* **1982**, *257*, 3669.
[20] A. Lawrence, C. M. Jones, P. Wardman, M. J. Burkitt, *J. Biol. Chem.* **2003**, *278*, 29410.

Received: February 1, 2012
Published online: March 21, 2012

